CHINA FOUNDRY Research & Development
Vol. 20 No. 4 July 2023
www.springer.com/41230
https://doi.org/10.1007/s41230-023-2187-2

Study on anisotropy of microstructure and mechanical properties of AZ31 magnesium alloy fabricated by wire arc additive manufacturing

Dong Ma[1, 2, 3], *Chun-jie Xu[1, 2, 3], Jun Tian[2, 4], Shang Sui[1, 2, 3], Can Guo[1, 2, 3], Xiang-quan Wu[1, 2, 3], and Zhong-ming Zhang[1, 2, 3]

1. School of Materials Science and Engineering, Xi'an University of Technology, Xi'an 710048, China

2. Xi'an Shechtman Nobel Prize New Materials Institute, Xi'an 710048, China

3. Xi'an Key Laboratory of Advanced Magnesium Alloy Additive Manufacturing and Precision Forming, Xi'an 710048, China

4. MGM Nobel Prize New Materials Co., Ltd., Tongchuan 727100, Shaanxi, China

Abstract: Based on wire arc additive manufacturing (WAAM) technology, AZ31 magnesium alloy in bulk was successfully fabricated, and its microstructure as well as mechanical properties in different planes were observed and analyzed. The AZ31 magnesium alloy has a similar microstructure in the building direction (*Z*) and travel direction (*X*), both of which are equiaxed grains. There are heat-affected zones (HAZs) with coarse grains below the fusion line. The second phase is primarily composed of the $Mg_{17}Al_{12}$ phase, which is evenly distributed in different directions. In addition, the residual stress varies in different directions. There is no significant difference in the hardness of the AZ31 alloy along the *Z* and *X* directions, with the average hardness being 68.4 HV and 67.9 HV, respectively. Even though the specimens' ultimate tensile strength along the travel direction is higher in comparison to that along the building direction, their differences in elongation and yield strength are smaller, indicating that the anisotropy of the mechanical properties of the material is small.

Keywords: magnesium alloy; wire arc additive manufacturing; anisotropy; microstructure; mechanical properties

CLC numbers: TG146.22 **Document code:** A **Article ID:** 1672-6421(2023)04-280-09

1 Introduction

Magnesium and its alloys, being the lightest engineering metal materials, possess the advantages of high specific strength and stiffness, superior electromagnetic shielding performance, and good vibration resistance [1-4]. With the rapid advancement of the modern aerospace and rail transportation industries, there is an urgent need for Mg alloys with a suitable combination of mechanical properties and complex structures [5, 6]. Nevertheless, restricted by the Mg alloy inherent nature of the hexagonal close-packed (HCP) structure, fabricating Mg alloy parts with complex structures by casting is difficult due to numerous casting defects, poor mechanical properties, long production cycles, and other associated problems [7-9]. Adopting innovative manufacturing techniques is urgently needed to further expand the commercial application of magnesium alloys. Wire arc additive manufacturing (WAAM) is a technology that uses a layer-by-layer method to manufacture alloy components. The metal wire was employed as the raw material and an arc was selected as the heat source, which has the benefit of low cost, high efficiency, and almost no limitation on the size of formed components [10-12]. As a result, WAAM has a significant application value and is particularly well-suited for producing lightweight and complexly structured products.

The WAAM of magnesium alloy is now the subject of research by both domestic and foreign scholars. Fang et al. [13] used tungsten argon arc welding (GTA) to fabricate a thin-walled AZ31 magnesium alloy component with finely equiaxed grains. The average grain size was about 24.7 μm and both of its ultimate tensile strength and yield strength were close to the

***Chun-jie Xu**

Male, born in 1971, Professor. He has been working in the field of metallic materials preparation and their composites. In particular, his research interests mainly focus on developing new preparation techniques to expand the applications of metallic materials. To date, he has published more than 180 papers.

E-mail: xuchunjie@xaut.edu.cn

Received: 2022-12-28; Accepted: 2023-06-12

level of forged AZ31. The impact of heat source parameters of cold metal transfer (CMT) on the formability of the AZ31 magnesium alloy was examined by Wang et al. [14]. The findings revealed that the appropriate CMT welding parameters can make it possible to achieve a wide and shallow deposited weld bead with excellent wettability and lower equivalent heat input. Guo et al. [15] investigated the formability of the AZ80M magnesium alloy. The results showed that the width of the thin wall initially increased before remaining stable; the top zone, middle zone and bottom zone of the thin wall had obvious differences in microstructure. Based on the layer-by-layer stacking process of WAAM, the magnesium alloy component exhibited a multilayered structure with alternating arc zones and melt pool boundaries along the building direction. This was related to the local thermal gradient during the deposition process and caused the size of grains to change continuously [16, 17]. The mechanical characteristics of the magnesium alloy workpiece may be significantly influenced by the non-equilibrium microstructure of the material. Moreover, the anisotropy of microstructure and mechanical properties has yet to be systematically studied and there are currently just a few relevant studies on WAAM Mg alloy components. Thus, a detailed discussion on the anisotropy in various planes of the microstructure and mechanical characteristics of the Mg alloy component is essential.

In this study, a 15-layer AZ31 block specimen was fabricated by cold metal transfer-based wire arc additive manufacturing technology (WAAM-CMT). The retracting wire makes it easier for a droplet to separate during a short circuit and transfer into a molten pool without the need for electromagnetic force during the CMT process, and the heat input is greatly reduced. In addition, the anisotropy of microstructure and mechanical properties of AZ31 was systematically examined and summarized. This will provide guidance for the manufacture of magnesium alloy components with complex structures and exceptional properties.

2 Experimental produce

The equipment for this experiment was primarily composed of a Fronius CMT Advanced 4000R welding machine and a six-axis ABB industrial robot. On the AZ31 magnesium alloy substrate with dimensions of 200 mm × 150 mm × 20 mm, the AZ31 magnesium alloy (Mg-2.99Al-0.87Zn-0.22Mn, wt.%) welding wire with a diameter of Φ1.2 mm was utilized as an arc additive filling material. Prior to the experiment, the substrate was firstly cleaned with acetone to remove impurities on its surface, followed by cleaning with ethanol. Moreover, the substrate was preheated to 160 °C before depositing. Throughout the experiment, the flow rate of the shielding gas (high-purity argon) of the welding gun tip was kept at 18 L·min^{-1}, and there was a 10 mm distance between the welding gun tip and the workpiece.

On the basis of the preliminary experimental results, various parameters of the CMT manufacturing process are presented in Table 1. To reduce heat accumulation, an interlayer dwell time of 180 s was implemented between each deposited layers. The residual oxide on the surface of each deposited layer was eliminated during the interlayer dwell period. Using the aforementioned welding parameters, a magnesium alloy block with a length of 150 mm, a width of 50 mm and a height of 60 mm was fabricated layer by layer. Moreover, a reference coordinate system was established in which the *X*-axis represented the travel direction, the *Z*-axis indicated the building direction, and the *Y*-axis was perpendicular to the travel direction, as shown in Figs. 1(a) and (b).

Table 1: Characteristic parameters for deposition of AZ31 magnesium alloy

Parameter	Value
Boost current, I_{boost} (A)	230
Boost voltage, V_{boost} (V)	18
Boost current time, $t_{I\,boost}$ (ms)	3
Short circuit current, $I_{sc\,wait}$ (A)	35
Short circuit voltage, $V_{sc\,wait}$ (V)	5
Short circuit current time, $t_{I\,sc\,wait}$ (ms)	7
Wire feed speed (m·min^{-1})	9
Travel speed (mm·s^{-1})	7

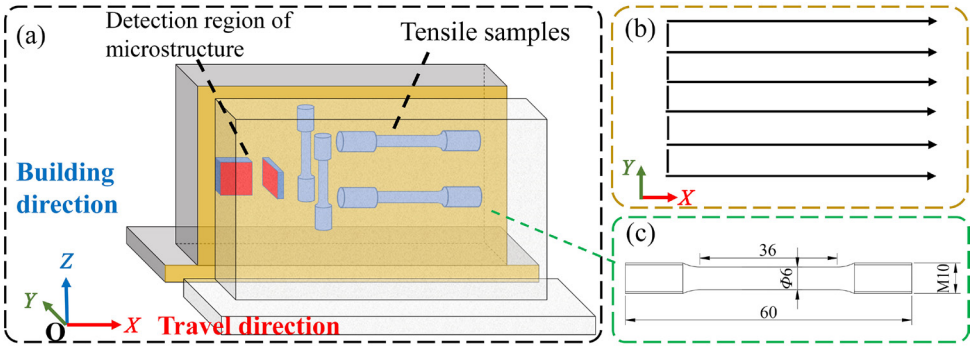

Fig. 1: View of the block component with the illustration of microstructure and tensile test specimens (a), the reciprocating unidirectional strategy (b), and the geometry of tensile specimens (c)

For microstructure analysis, electric discharge wire cutting was used to cut specimens from the AZ31 alloy block along the *YOZ* and *XOZ* planes. The sampling location and observation surface are shown in Fig. 1(a). The specimens used for metallographic analysis were firstly prepared by mechanical polishing, which were then immediately etched with a 4% nitric acid solution for 10 s to 20 s. Using an Olympus GX51 optical microscope, the microstructural structures of the specimens were observed. The second phase content was calculated by ImageJ software. Scanning electron microscopy (SEM) analysis adopted a TESCAN VEGA3 XUM scanning electron microscope equipped with an ELEMENT energy spectrometer as well as Oxford EBSD system and Channel 5 software so as to further characterize the grain morphology of the CMT-AZ31 specimens. An HV-120 Vickers hardness tester was used to measure the specimens' Vickers hardness. The test load was 5 N and the loading time was 15 s. The test position was selected along the building direction (*Z*) with a spacing of 2 mm and the travel direction (*X*) with a spacing of 5 mm. The trend in hardness was determined using the data point fitting technique. The tensile test was carried out on the AZ31 block along the building direction and the travel direction by the HT-2402 computer servo-controlled material testing machine at a tensile speed of 1 mm·min^{-1}. Figure 1(c) shows the dimension of the tensile specimen. The corresponding fracture morphologies of the tensile specimens were investigated by SEM.

3 Results and discussion

3.1 Microstructure analysis

Figure 2(a) shows the 15-layer AZ31 magnesium alloy component fabricated via the WAAM process. The magnesium alloy component shows consistent similar layer heights throughout, exhibiting a layered accumulation morphology. There is no collapse, serious cracks or other defects on the surface of the part, demonstrating that the workpiece has good formability. There are, nevertheless, some metal droplet overflows on the middle part of the bulk surface, which is due to the poor stability of the arc droplet during the deposition process. Since the interlayer dwell time between two adjacent deposition layers is as long as 180 s, less heat is accumulated in the material, which also reduces the flow of liquid droplets. Moreover, a very small amount of droplet overflow has no necessary negative impact on the component formability. Figure 2(b) shows the partial macroscopic morphology of the AZ31 specimen along the building direction. As can be observed, the overall surface of the component is uniform and scale-like, and the fusion height and width of each layer are about 5 mm and 4 mm, respectively. The fusion line of the *YOZ* plane presents multiple quadrilateral stacked shapes. In comparison to the 2–3 mm melting height of a single layer in the conventional WAAM process [16, 18], the adjacent deposition passes in this experiment overlapped each other with a certain inclination angle, hence, the melting height is higher. Furthermore, the adjacent deposition layers are closely arranged and no obvious pores or hot crack defects are found.

Figure 3 displays the microstructures of the AZ31 alloy specimen on the *XOZ* plane and *YOZ* plane. The deposited zones (DZ) are all made up of equiaxed crystals, as can be observed in Figs. 3(a) and (b), and the microstructures in various directions are comparable. The fusion lines can be clearly observed between the DZs, while below [Fig. 3(a)], or to the right [Fig. 3(b)], the fusion line is the heat-affected zone (HAZ). The HAZ in Fig. 3(a) is in the shape of a thin band that has a thickness of about 240 μm in the *XOZ* plane. However, the extent of the HAZ is not obvious in the *YOZ* plane, as shown in Fig. 3(b). There are some variations in the size of equiaxed grains in different zones of the same plane. Due to the in-situ heat treatment impact on the preceding layer caused by the deposition of the current layer, the grains in the HAZ expand substantially more than those in the bottom area of the DZ. During the deposition process, the grains in the top region of each deposited layer simultaneously receive a significant quantity of heat input from the arc source. Although the excessive heat input does not melt all the grains at the top of the previous layer, it still has a considerable effect on some grain sizes [19]. This in-situ heat treatment effect of the deposition of the current layer on the previous layer eventually leads to a notable increase in grain size in the top region of each deposited layer. As a result, a few coarse grains appear in

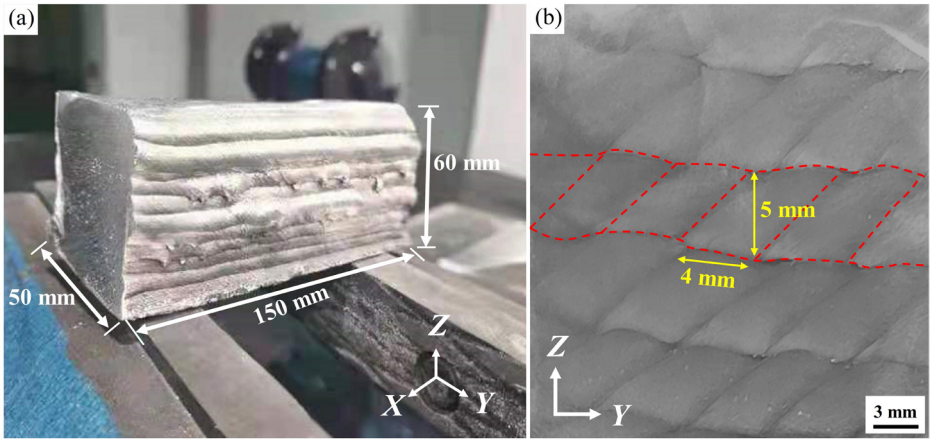

Fig. 2: Macrostructures of WAAM AZ31 magnesium alloy: (a) external view; (b) *YOZ* cross-section

the upper part of the deposited layer. Fine grains, nevertheless, still dominate in the entire deposited layers. In addition, the second phases in the microstructure are evenly distributed without segregation (purple circles), as depicted in Figs. 3(a_2) and (b_2). The area fraction of the second phase in the *XOZ* and *YOZ* planes was computed using ImageJ software, yielding results of 10.4%±2.1% and 9.8%±3.6%, respectively. The content of the second phase on different planes is basically the same. Besides, a very small amount of micropores (orange arrows) are found in both the DZ and the HAZ, and these micropores might serve as the starting points of crack propagation [13, 17].

It is worth noting that the grain growth direction in different planes is not clearly defined along the building direction, and that no columnar crystals are formed. Firstly, this is due to the good heat dissipation capability of magnesium alloy and the low heat input in CMT mode [20, 21]. In general, the morphology is controlled by the grain growth rate to temperature gradient ratio (G/R), while the crystal growth is governed by the $G\times R$ product. The microstructure may switch from a dendritic to an equiaxed one as constitutional undercooling increases [13]. The higher the cooling rate and nucleation rate, the finer the grains. In this experiment, the calculation of heat input in CMT mode could be expressed in accordance with the heat input (HI). The studies of Cong et al. [22] and Pang et al. [23] gave similar calculation equations for heat input:

$$\mathrm{HI}=\frac{\int_{t_1}^{t_2}U_iI_i\mathrm{d}t}{t_2-t_1}/v \tag{1}$$

where I_i and U_i represent the instantaneous currents and instantaneous voltages, respectively. v denotes the welding speed, and t_1 and t_2 represent the start and end times respectively of a certain stage in the arc-starting process. The single-cycle heat input of the CMT arc in this experiment could be computed using Eq. (1) to be 194.9 J·mm^{-1}, which is lower in comparison to the conventional CMT+pulse (P), gas tungsten arc welding (GTAW), and other arc heat source manufacturing modes [24]. The lower heat input reduces crystallization latent heat, leading to an increase in the number of nucleations and the formation of finer equiaxed grains. Secondly, due to the long interlayer dwell time in this experiment, the original heat accumulation in the specimen is effectively reduced. Therefore, it is difficult for grains to grow continuously in the deposited region, resulting in a predominantly equiaxed microstructure.

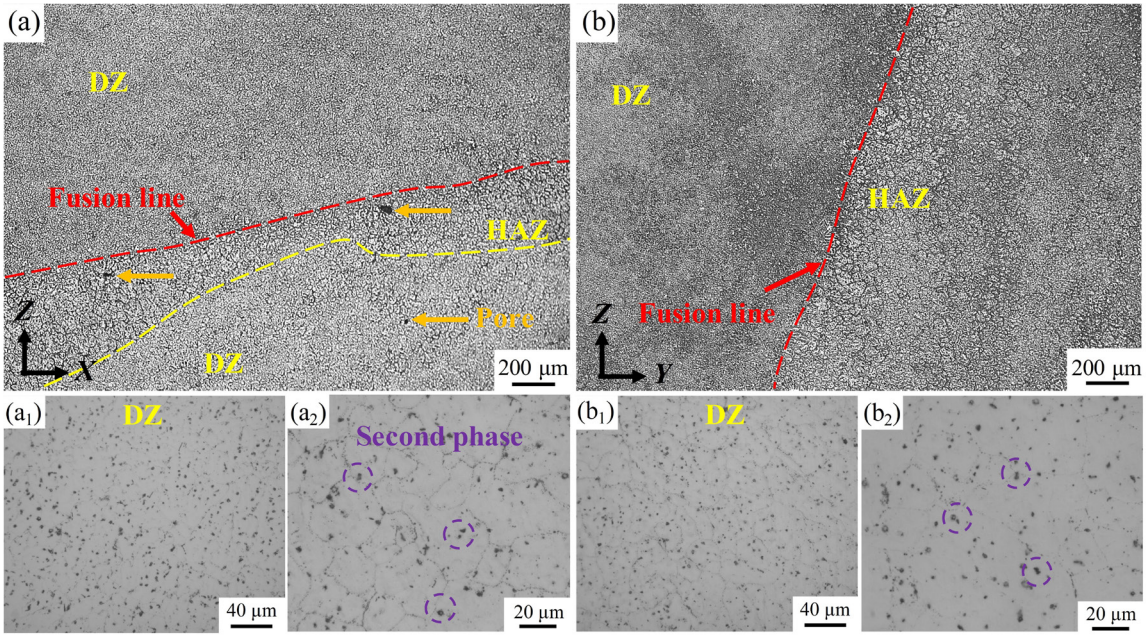

Fig. 3: Microstructures of WAAM AZ31 magnesium alloy: (a, a_1, a_2) *XOZ* plane; (b, b_1, b_2) *YOZ* plane

Figure 4 highlights the SEM image of the AZ31 alloy specimens on the *XOZ* plane and *YOZ* plane. The microstructure of specimens in various directions is primarily made up of α-Mg and a small amount of $Mg_{17}Al_{12}$ phases. The $Mg_{17}Al_{12}$ phases with a granular morphology are evenly distributed on the matrix. In addition, $Mg_{17}Al_{12}$ phases are smaller in size in the HAZ [Fig. 4(a)]. This is caused by the high heat input in the HAZ, which is more conducive to the diffusion of element while promoting the dispersed distribution of the $Mg_{17}Al_{12}$ phase.

EBSD analysis of the AZ31 alloy specimens that are parallel to the *XOZ* and *YOZ* planes, is depicted in Fig. 5. On different planes of the AZ31 alloy, there are relatively uniform equiaxed grains with varying crystal orientations, and no obvious columnar grains can be found [Figs. 5(a) and (b)]. The specimen with the *XOZ* plane has an average grain size of 22.4 μm [Fig. 5(a_2)], which is basically the same as the specimen on the *YOZ* plane (22.9 μm), in Fig. 5(b_2). Furthermore, kernel average misorientation (KAM) maps are produced from the EBSD data, as illustrated in Figs. 5(a_1) and (b_1). It is widely

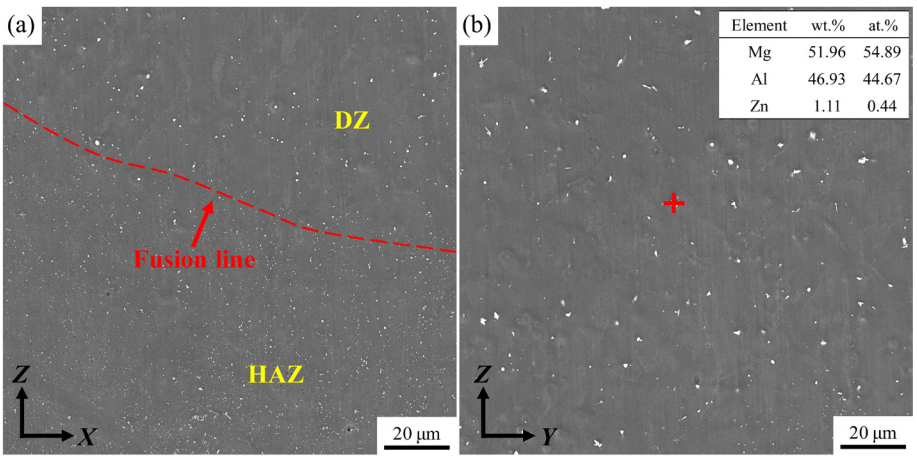

Fig. 4: SEM images of WAAM AZ31 magnesium alloy: (a) *XOZ* plane; (b) *YOZ* plane

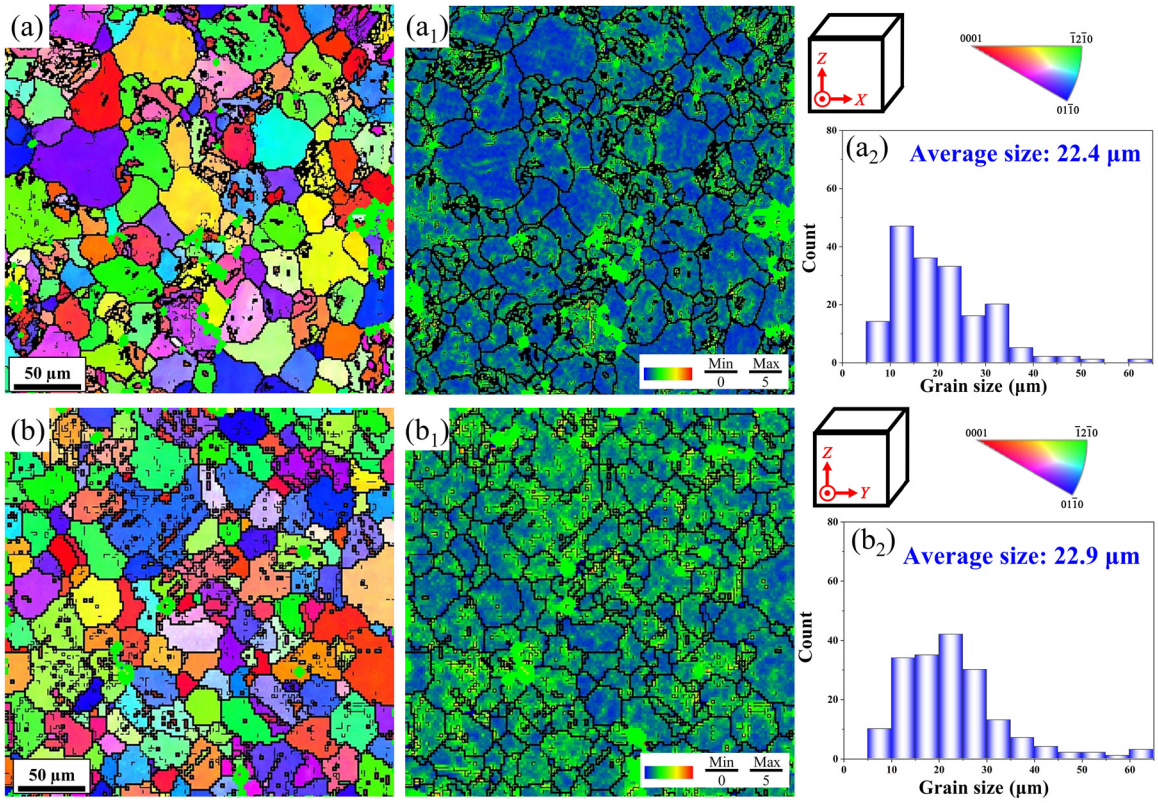

Fig. 5: EBSD scan images of specimen at *XOZ* (a, a_1, a_2) and *YOZ* (b, b_1, b_2) planes: (a, b) inverse pole figure; (a_1, b_1) KAM maps; (a_2, b_2) grain size distribution

known that a KAM map offers an average misorientation around the measurement point and is a good qualitative indicator of dislocations [25]. Thus, the residual stress can be described indirectly by KAM maps [26]. The KAM map of the specimen in the *XOZ* plane shows mostly dark blue, demonstrating that there are few dislocations and low residual stress [Fig. 5(a_1)]. The residual stress of the specimen is greater on the *YOZ* plane, as can be observed from the light green region of the KAM map [Fig. 5(b_1)].

The AZ31 magnesium bulk material was fabricated by multi-channel and multi-layer paths in this experiment. As a result, stacking modes of the various planes vary, leading to significant changes in residual stress. On the *XOZ* plane, the traveling path of the welding torch is along the *X* direction, the fusion lines are in a parallel state, and the number of fusion lines is small [Fig. 6(a)]. On the *YOZ* plane, the welding torch is firstly stacked along *Y* direction at the same height for multiple passes. After the completion of the multi-channel deposition layers, a single multi-pass accumulation was performed at a increased height. Hence, the fusion line of the *YOZ* plane also presents multiple quadrilateral stacked shapes, and the number of fusion lines is corresponding increased [Fig. 6(b)]. More fusion lines imply that the plane has experienced multiple heating and cooling cycles, which has a greater impact on the deposited layer [27]. The residual stress in the specimen of the *YOZ* plane is thus higher than that in the specimen of the *XOZ* plane.

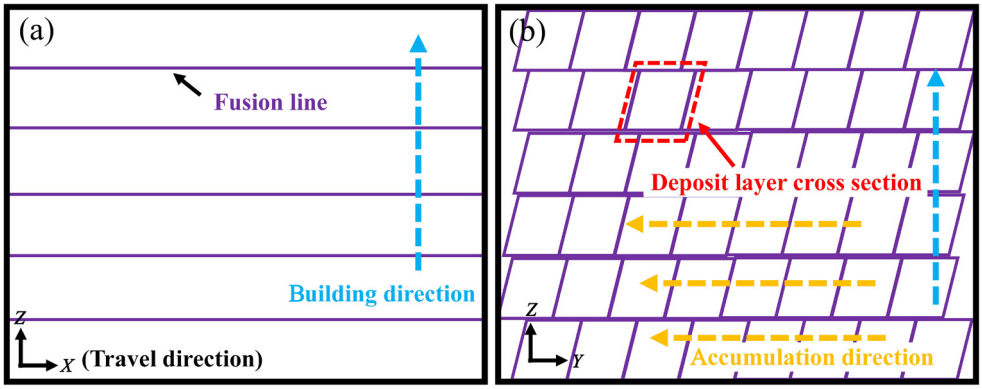

Fig. 6: Schematic diagram of different planes of WAAM AZ31 magnesium alloy: (a) *XOZ* plane; (b) *YOZ* plane

In addition, Fig. 7 displays the pole figure of the AZ31 alloy component on different planes. It can be seen that there is a weak basal texture {0001} in all planes. The maximum multiples of uniform distribution (MUD) value of the *XOZ* plane specimen is 5.04, as indicated in Fig. 7(a). While, there exists a typical basal texture with a maximum MUD value of 8.22 for the *YOZ* plane specimen [Fig. 7(b)], which is higher than the *XOZ* plane specimen. Generally, finer grains result from higher cooling and nucleation rates. In this experiment, the arc source used cold material transfer technology, the retracted wire makes it easier for droplets to detach during a short circuit and transfer into the molten pool without relying on electromagnetic force during the CMT process. This reduces heat input and eliminates spattering issues. Therefore, it is conducive to the formation of equiaxed grains. As a result of the equiaxed-grain-dominated microstructure in the thin-wall component, the microstructure is found to be essentially the same and exhibits no anisotropy trend in the metallography and EBSD morphology of the *XOZ* and *YOZ* planes.

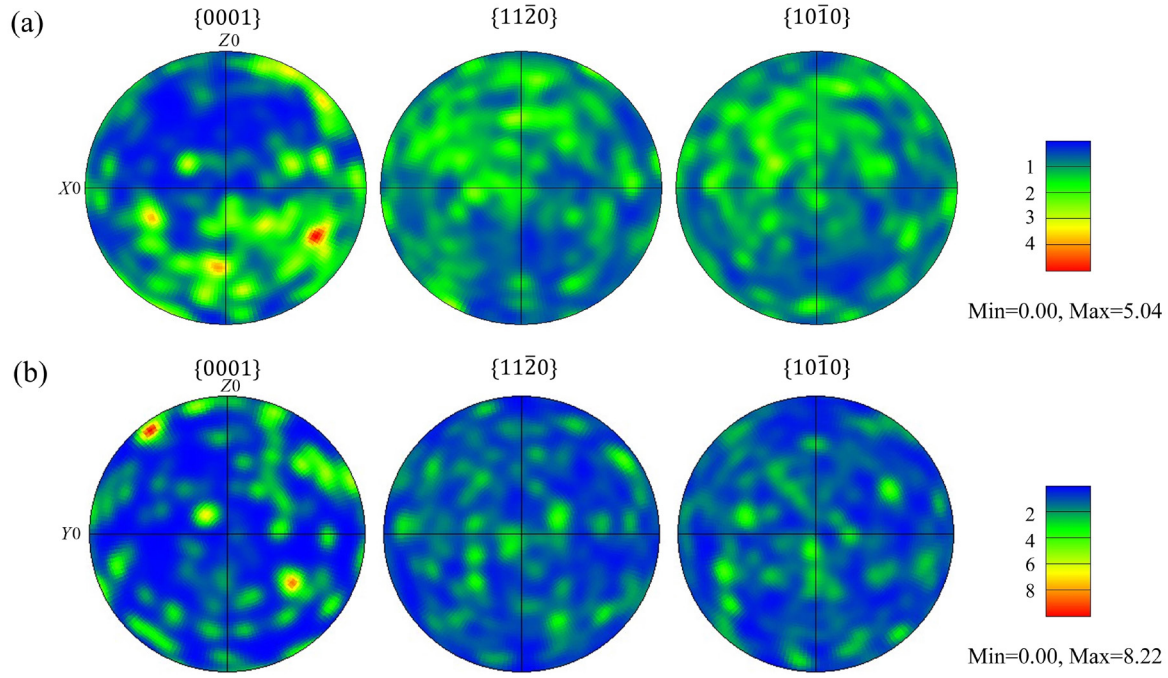

Fig. 7: Pole figures of *XOZ* (a) and *YOZ* (b) planes of WAAM AZ31 magnesium alloy

3.2 Mechanical properties

Figure 8 depicts the Vickers microhardness distribution of the AZ31 magnesium alloy. Figure 8(a) shows the microhardness distribution along the building direction is relatively uniform, with an average microhardness value of 68.4 HV. The trend of microhardness change is not obvious and it can be considered that the microhardness basically remains unchanged with the increase in height. Figure 8(b) shows the distribution of microhardness along the travel direction of the welding torch. The distribution fluctuates less, and the microhardness tends to decrease slightly from the beginning to the end and has an average microhardness value of 67.9 HV. The difference in microhardness is mostly related to grain size, and heat input directly affects grain size. Increasing the heat input makes

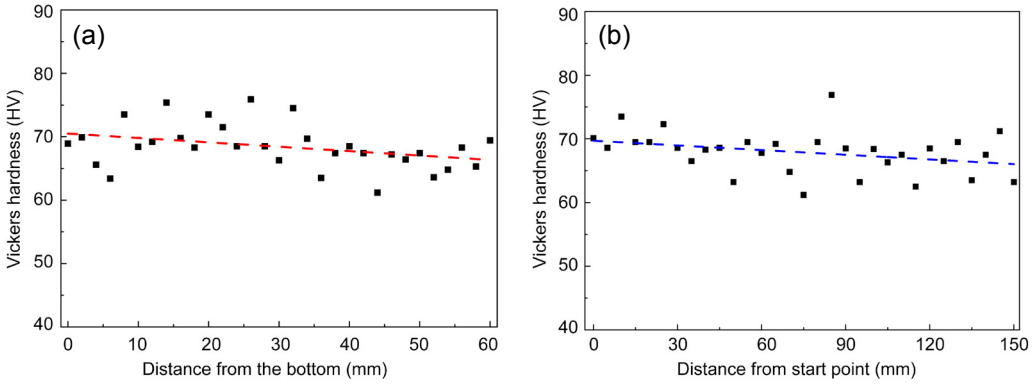

Fig. 8: Microhardness of the AZ31 magnesium alloy: (a) building direction (*Z*); (b) travel direction (*X*)

it easier to form coarse grains, resulting in a reduction in microhardness. In contrast, decreasing heat input tends to reduce the grain size and increase the microhardness value [28]. Due to the application of the CMT mode with a low heat input in this experiment, the grain size of the AZ31 alloy component is uniform and small on both directions, resulting in a high microhardness value with little variation.

The tensile engineering stress-strain curves at room temperature for the AZ31 component along the building direction and the travel direction are presented in Fig. 9. Table 2 summarizes the room temperature tensile properties of the AZ31 alloys along different directions. The best mechanical properties of AZ31 alloy along the *X* direction are that the yield strength (YS), ultimate tensile strength (UTS) and elongation (EL) are 110 MPa, 245 MPa and 23.6%, respectively. It can be easily inferred from Table 2 that the tensile strength of the AZ31 alloys along the *X* direction, in particular the UTS, is better when compared to the specimens along the *Z* direction. However, when it comes to EL and YS, the difference between the specimens along the different directions is small. The variation in mechanical properties is caused by disparity in microstructure. Based on the layer-by-layer accumulation technology of wire arc additive manufacturing, the thin-wall component has a clear layered microstructure. In the HAZ between layers, coarse grains and some micro-pores and micro-cracks are produced, as shown in Fig. 3, which reduce the tensile properties [13, 15]. It can be seen that the number of HAZ of the *XOZ* plane is less than that of the *YOZ* plane due to the difference in deposition path in Fig. 6. Thus, in contrast to the tensile specimens along the *X* direction, the microstructure along the *Z* direction contains more heat-affected zones, which means that there are more defects and, thus, causes a decrease in mechanical properties. Despite this, it can be said that there is very little change in the tensile mechanical characteristics between the different deposition orientations, suggesting that the anisotropy of the mechanical properties of the specimens is not obvious.

Figure 10 shows the room temperature tensile fracture morphologies of the AZ31 magnesium alloys along different directions. Similar to a typical ductile fracture, it consists of a large number of irregularly distributed dimples and uneven grid-like tearing edges. It complies with the isotropic

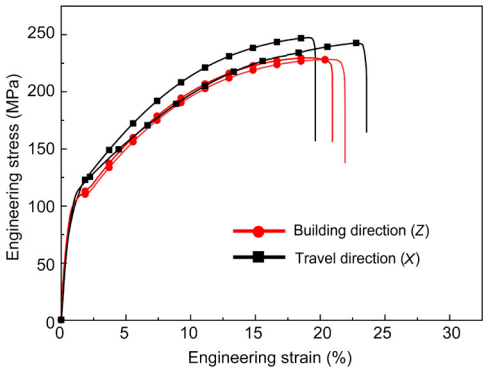

Fig. 9: Representative tensile engineering stress-strain curves of AZ31 alloys under different directions

Table 2: Room temperature tensile properties of AZ31 alloys under different directions

Specimen types	YS (MPa)	UTS (MPa)	EL (%)
Building direction, *Z*	99	228	22.3
	101	230	20.9
Travel direction, *X*	100	248	19.7
	110	245	23.6

tensile properties and the layer characteristics within the microstructure. The fracture along the *X* direction has more dimples than the fracture along the *Z* direction. This also means that the AZ31 alloys have better mechanical properties along the *X* direction.

4 Conclusions

In this experiment, the AZ31 magnesium alloy block fabricated by the WAAM-CMT technology exhibits good formability and shows no evident defects. Its microstructure as well as mechanical properties have been investigated and analyzed. The following are the main conclusions:

(1) The microstructures of different planes of the AZ31 magnesium alloy are mainly composed of equiaxed grains with varying sizes, and the heat-affected zones are below the fusion line. The grain size in the heat-affected zone is larger. In addition, the AZ31 alloy component has a very small amount of micropores.

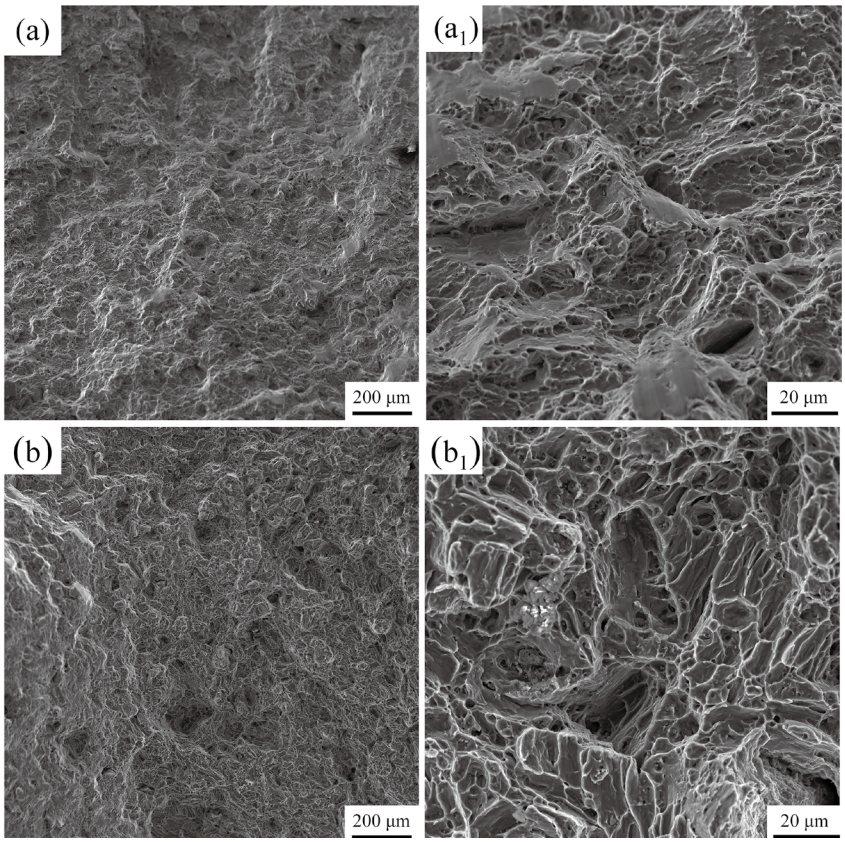

Fig. 10: Room temperature tensile fracture morphologies of AZ31 alloys along different directions: (a, a_1) building direction; (b, b_1) travel direction

(2) The microstructure of AZ31 magnesium alloy is mainly composed of α-Mg matrix and $Mg_{17}Al_{12}$ phase, with the second phases being evenly distributed. The grain size of the *XOZ* plane is comparable to that of the *YOZ* plane. Moreover, the specimen on the *YOZ* plane has higher residual stress.

(3) No significant difference exists in the microhardness of AZ31 magnesium alloy along the building direction and travel direction, and the average hardness is 68.4 HV and 67.9 HV, respectively. The building direction has higher tensile strength, nonetheless, the difference between elongation and yield strength is small. This points out that the anisotropy of the mechanical properties of the material is small. The fractures of tensile specimens are all ductile fractures.

Acknowledgements

The authors would like to acknowledge the support from the International Science and Technology Cooperation Program of Shaanxi Province (No. 2023-GHZD-50), Projects of Major Innovation Platforms for Scientific and Technological and Local Transformation of Scientific and Technological Achievements of Xi'an (No. 20GXSF0003), Projects of Major Scientific and Technological Achievements Local Transformation of Xi'an (No. 2022JH-ZDZH-0039), and the Higher Education Institution Discipline Innovation and Intelligence Base of Shaanxi Province (No. S2021-ZC-GXYZ-0011).

Conflict of interest

The authors declare that they have no known competing financial interests or personal relationships that could have appeared to influence the work reported in this paper.

References

[1] Song J F, Chen J, Xiong X M, et al. Research advances in magnesium and magnesium alloys worldwide in 2021. Journal of Magnesium and Alloys, 2021, 10(4): 863–898.
[2] Srinivas A, Pavan D, Venkatesha B K, et al. Study on mechanical properties of AZ91 magnesium alloy. Materials Today: Proceedings, 2022, 54: 291–294.
[3] Zheng D D, Li Z, Jiang Y L, et al. Effect of multiple thermal cycles on the microstructure evolution of GA151K alloy fabricated by laser-directed energy deposition. Additive Manufacturing, 2022, 57: 102957.
[4] Li F F, Fang G. Stress-state dependency of ductile fracture in an extruded magnesium alloy and its underlying mechanisms. International Journal of Plasticity, 2022, 152: 103258.
[5] Zhang W G, Li K, Chi R Q, et al. Insights into microstructural evolution and deformation behaviors of a gradient textured AZ31B Mg alloy plate under hypervelocity impact. Journal of Materials Science and Technology, 2021, 91: 40–57.
[6] Yang Y, Xiong X M, Chen J, et al. Research advances in magnesium and magnesium alloys worldwide in 2020. Journal of Magnesium and Alloys, 2021, 9(3): 705–747.
[7] Hou Y Y, Wu M W, Huang F. Defect band formation in high pressure die casting AE44 magnesium alloy. China Foundry, 2022, 19(3): 201–210.

[8] Wang D, Fu P H, Peng L M, et al. Development of high strength sand cast Mg-Gd-Zn alloy by co-precipitation of the prismatic β′ and β_1 phases. Materials Characterization, 2019, 153: 157–168.
[9] Weiler J P. A review of magnesium die-castings for closure applications. Journal of Magnesium and Alloys, 2019, 7(2): 297–304.
[10] Langi E, Zhao L G, Jamshidi P, et al. A comparative study of microstructures and nanomechanical properties of additively manufactured and commercial metallic stents. Materials Today Communications, 2022, 31: 103372.
[11] Oliveira J P, Santos T G, Miranda R M. Revisiting fundamental welding concepts to improve additive manufacturing: From theory to practice. Progress in Materials Science, 2020, 107: 100590.
[12] Treutler K, Wesling V. The current state of research of wire arc additive manufacturing (WAAM): A review. Applied Sciences, 2021, 11(18): 1–54.
[13] Fang X W, Yang J N, Wang S P, et al. Additive manufacturing of high performance AZ31 magnesium alloy with full equiaxed grains: Microstructure, mechanical property, and electromechanical corrosion performance. Journal of Materials Processing Technology, 2022, 300: 117430.
[14] Wang P, Zhang H Z, Zhu H, et al. Wire-arc additive manufacturing of AZ31 magnesium alloy fabricated by cold metal transfer heat source: Processing, microstructure, and mechanical behavior. Journal of Materials Processing Technology, 2021, 288: 116895.
[15] Guo Y Y, Quan G F, Jiang Y L, et al. Formability, microstructure evolution and mechanical properties of wire arc additively manufactured AZ80M magnesium alloy using gas tungsten arc welding. Journal of Magnesium and Alloys, 2021, 9(1): 192–201.
[16] Yang X, Liu J R, Wang Z N, et al. Microstructure and mechanical properties of wire and arc additive manufactured AZ31 magnesium alloy using cold metal transfer process. Materials Science and Engineering: A, 2020, 774: 138942.
[17] Li X Z, Zhang M G, Fang X W, et al. Improved strength-ductility synergy of directed energy deposited AZ31 magnesium alloy with cryogenic cooling mode. Virtual and Physical Prototyping, 2023, 18: 1–22.
[18] Rosli N A, Alkahari M R, Abdollah M F B, et al. Review on effect of heat input for wire arc additive manufacturing process. Journal of Materials Research and Technology, 2021, 11: 2127–2145.
[19] Miao Q Y, Wu D J, Chai D S, et al. Comparative study of microstructure evaluation and mechanical properties of 4043 aluminum alloy fabricated by wire-based additive manufacturing. Materials and Design, 2020, 186: 108205.
[20] Chen F R, Yang Y H, Feng H L. Regional control and optimization of heat input during CMT by wire arc additive manufacturing: Modeling and microstructure effects. Materials, 2021, 14(5): 1–12.
[21] Zhang H, Hu S S, Wang Z J, et al. The effect of welding speed on microstructures of cold metal transfer deposited AZ31 magnesium alloy clad. Materials Design, 2015, 86: 894–901.
[22] Cong B Q, Ding J L, Williams S. Effect of arc mode in cold metal transfer process on porosity of additively manufactured Al-6.3%Cu alloy. The International Journal of Advanced Manufacturing Technology, 2015, 76(9): 1593–1606.
[23] Pang J, Hua S S, Shen J Q, et al. Arc characteristics and metal transfer behavior of CMT + P welding process. Journal of Materials Processing Technology, 2016, 238: 212–217.
[24] Srinivasan D, Sevvel P, Solomon I J, et al. A review on cold metal transfer (CMT) technology of welding. Materials Today: Proceedings, 2022, 64: 108–115.
[25] Birosca S, Liu G, Ding R G, et al. The dislocation behaviour and GND development in a nickel based superalloy during creep. International Journal of Plasticity, 2019, 118: 252–268.
[26] Liu D H, Wu D J, Wang R Z, et al. Formation mechanism of Al-Zn-Mg-Cu alloy fabricated by laser-arc hybrid additive manufacturing: Microstructure evaluation and mechanical properties. Additive Manufacturing, 2022, 50: 102554.
[27] Lopez-Sanchez M A, Tommasi A, Barou F, et al. Dislocation-driven recrystallization in AZ31B magnesium alloy imaged by quasi-in situ EBSD in annealing experiments. Materials Characterization, 2020, 165: 110382.
[28] Yuan T, Luo Z, Kou S. Mechanism of grain refining in AZ91 Mg welds by arc oscillation. Science and Technology of Welding and Joining, 2017, 22: 97–103.